Numerical Modelling of Reverse Combustion in a Fuel Bed of Pine Needles

D. MORVAN[1], B. PORTERIE[2], M. LARINI[2] and J.C. LORAUD[2]
[1] IRPHE UMR CNRS 6594
[2] IUSTI UMR CNRS 6595
Technopole de Chateau Gombert
13453 Marseille cedex 13 FRANCE

ABSTRACT

A one dimensional numerical model of reverse combustion is proposed to describe the physical mechanisms which control the fire spread in a fuel bed of pine needles. The physical model is constructed from a multiphase formulation, including various submodels to account for the main phenomena which contribute at different levels to fire spread. The set of partial differential equations which governs the physical behaviour of the gas flow and of the solid fuel bed is solved using a finite volume method associated with an adaptive mesh algorithm to track correctly the thin region where the thermal degradation of the solid fuel occurs. Both oxygen-limited and fuel-limited regimes are examined for inlet flow velocities ranging from 2 to $30cm/s$.

KEY WORDS: Reverse Combustion, Fire Spread, Radiative Heat Transfer, Porous Fuel Bed.

INTRODUCTION

The understanding of the physical mechanisms which control the ignition and the spread of wildland fires constitutes a major objective for the management and the preservation of forest areas. Various numerical models based on statistical, empirical or physical approach have been proposed to evaluate the spread velocity of a surface forest fire [1]. These simplified models allow to obtain a quite good approximation of the rate of spread of the fire as a function of the fuel load, the wind intensity and the terrain slope for particular conditions (close to experiments carried out for the calibration of the parameters used in such models). Unfortunately these models cannot be extended to other fire conditions. The main reason is that the physical mechanisms which control the thermal degradation of solid fuel, the fire behaviour and the solid-flame interactions are not (or very poorly) describeb in such models. These physical mechanisms are very complex since they include convection and radiation heat transfers between the two phases downstream the fire front which are responsible of the thermal degradation (pyrolysis) of the solid fuel and subsequently of the spread of the fire through the fuel bed [2].
To improve the quality of numerical predictions, a more complete approach based on a multiphase formulation can be adopted [3, 4, 5, 6, 7]. This formulation consists in describing the evolution of both phases. The coupling between the solid and the gaseous phase is rendered through source terms in the mass (decomposition of solid fuel to combustible gas), momentum (drag force), and energy (heat transfer by convection and radiation) balance equations. The solid phase is assimilated as a porous medium characterized by a porosity which varies during the fuel decomposition. In absence of wind, experimental investigations have shown that the heat flux necessary for sustaining a spreading fire is the result of convective (60%) and radiative (40%) heat transfers [2]. Though radiative heat transfer is not the dominant

mode for fire spread under windy conditions, it cannot be neglected. To evaluate the irradiance field related to the radiative heat flux, we have used the P1-approximation. This method is particularly adapted to solve coupled radiative and convective heat transfers in a gray gas [8, 9]. In the present paper the radiative contribution of soot and solid particles through the absorption coefficient is considered [4, 10]. The configuration used in the present study is represented in Figure 1. The fuel bed of pine needles (pinus pinaster) is confined in a horizontal tube. The is lit at one end of the tube and travels through it in the opposite direction as the oxidizer flow. In this case the effects of buoyancy can be neglected and the problem is limited to one dimension. This simplified configuration does not represent all the physical phenomena encountered during a surface fire (buoyancy effects, flame expansion above the flaming fuel bed ...) but it represents a very interesting case to assess the validity of the parameters introduced in the submodels used for the description of the thermal degradation of the solid fuel bed and the solid-gas interactions.

PHYSICAL MODEL AND NUMERICAL RESOLUTION

MATHEMATICAL FORMULATION

By using a multiphase approach [3, 4, 5, 6, 7] the mass, species, momentum, and energy conservation equations in the gas phase can be written as follows:

$$\frac{\partial}{\partial t}(\alpha_g \rho_g) + \frac{\partial}{\partial x}(\alpha_g \rho_g u_x) = \sum_\alpha \dot{M}_{s,\alpha} \tag{1}$$

$$\frac{\partial}{\partial t}(\alpha_g \rho_g Y_\alpha) + \frac{\partial}{\partial x}(\alpha_g \rho_g u_x Y_\alpha) = \frac{\partial}{\partial x}\left(\alpha_g \rho_g \mathcal{D}_\alpha \frac{\partial Y_\alpha}{\partial x}\right) + \dot{\omega}_\alpha + \dot{M}_{s,\alpha} \tag{2}$$

$$\frac{\partial}{\partial t}(\alpha_g \rho_g u_x) + \frac{\partial}{\partial x}(\alpha_g \rho_g u_x^2) = \frac{\partial}{\partial x}(\alpha_g(\sigma_{xx} + \sigma_{xy})) - \frac{3}{8}\alpha_g \rho_g C_d |u_x| u_x \Sigma_s \tag{3}$$

$$\frac{\partial}{\partial t}(\alpha_g \rho_g h) + \frac{\partial}{\partial x}(\alpha_g \rho_g u_x h) = \frac{\partial}{\partial x}\left(\alpha_g k_g \frac{\partial T}{\partial x}\right) - h_{cond}\Sigma_s(T - T_s) \tag{4}$$

$$+\frac{\partial}{\partial t}(\alpha_g p) - \frac{\partial}{\partial x}(\alpha_g q_x^R) + \sum_\alpha \dot{M}_{s,\alpha} h_{s,\alpha}$$

where α_g, ρ_g, u_x, Y_α, $\mathcal{D}_\alpha$, h are respectively the volume fraction, the density, the velocity, the mass fraction and the diffusion coefficient of species α, and the enthalpy of the gas mixture; p, $(\sigma_{xx}, \sigma_{xy})$, T, T_s, k_g, q_x^R are the pressure, the stress tensor components, the gas and the solid phase temperatures, the conductivity, and the radiative heat flux. The solid-gas interaction terms (drag, heat transfer [11] at the gas-particle interface) include naturally the corresponding surface density (Σ_s) which is a characteristic of the fuel bed (approximated as a randomly distributed cylinders).

Using the P1-approximation the radiative heat flux is evaluated solving the radiative transfer equation (RTE) including both the contribution of the soot-gas mixture and the solid fuel bed [4]:

$$\frac{\partial}{\partial x}\left(\frac{\alpha_g}{3\widetilde{a_R}}\frac{\partial}{\partial x}(\alpha_g J)\right) + \alpha_g a_R(4n^2\sigma T^4 - J) + \frac{\alpha_s \sigma_s}{4}(4n^2\sigma T_s^4 - J) = 0 \tag{5}$$

$$-\frac{\partial}{\partial x}(\alpha_g q_x^R) = \frac{\partial}{\partial x}\left(\frac{\alpha_g}{3\widetilde{a_R}}\frac{\partial}{\partial x}(\alpha_g J)\right) \tag{6}$$

$$\widetilde{a_R} = \alpha_g a_R + \frac{\alpha_s \sigma_s}{4} \quad \text{with} \quad a_R = 0.1 X_{Pro} + 1862 f_v \quad (m^{-1}) \tag{7}$$

where J, a_R and σ_s are the irradiance, the absorption coefficient of the soot/gas mixture and the surface to volume ratio of the solid particles which compose the fuel bed; X_{Pro} and f_v design the mole fraction of combustion products (CO_2 and H_2O) and the soot volume fraction, respectively.

The heat transfer from the combustion region to the fuel bed induces first the desorption of water then its degradation (by pyrolysis and oxidation) in combustible and uncombustible gases (essentially CO, CH_4, H_2, CO_2 [4]), char, soot, and ashes [4, 12, 13]. If the incandescent char particles are in contact with oxygen, a surface heterogeneous combustion occurs. Two-step reaction mechanism for pyrolysis, char formation and oxidation is assumed:

$$Solid \quad Fuel \rightarrow \nu_{char}\,(Char + Soot) + (1 - \nu_{char})\,CO \tag{8}$$

$$Char + \nu_{O_2} O_2 \rightarrow (1 + \nu_{O_2})\,CO_2 \tag{9}$$

$$\dot{\omega}_{pyr} = k_{pyr}\alpha_s \rho_s Y_i^s \exp\left[\frac{-E_{pyr}}{RT_s}\right] \tag{10}$$

$$\dot{\omega}_{H_2O} = \frac{k_{H_2O}}{\sqrt{T_s}}\alpha_s \rho_s Y_{H_2O}^s \exp\left[\frac{-E_{H_2O}}{RT_s}\right] \tag{11}$$

$$\dot{\omega}_{char} = \frac{M_C}{M_{O_2}} k_{char}\alpha_g \rho_g Y_{O_2} \exp\left[\frac{-E_{char}}{RT_s}\right] \Sigma_s \tag{12}$$

The preexponential factors and the activation energies are evaluated from experimental data obtained by thermogravimetry [4, 14]: $k_{pyr} = 8\ 10^4 s^{-1}$, $E_{pyr}/R = 9400\ K$, $k_{H_2O} = 6.05\ 10^5 K^{1/2} s^{-1}$, $E_{H_2O}/R = 5956\ K$, $k_{char} = 900\ m/s$, $E_{char}/R = 10^4\ K$.
The evolution of the mass fractions of solid fuel, water and char, the mass loss and the energy equation in the fuel bed can be evaluated from the following set of coupled differential equations:

$$\frac{d}{dt}(\alpha_s \rho_s Y_i^s) = -\dot{\omega}_{pyr} \tag{13}$$

$$\frac{d}{dt}(\alpha_s \rho_s Y_{H_2O}^s) = -\dot{\omega}_{H_2O} \tag{14}$$

$$\frac{d}{dt}(\alpha_s \rho_s Y_{char}^s) = (\nu_{char} - \nu_{soot})\,\dot{\omega}_{pyr} - \left(\frac{\nu_{ash}}{\nu_{char}} + 1\right)\dot{\omega}_{char} \tag{15}$$

$$\frac{d}{dt}(\alpha_s \rho_s) = -\sum_{\alpha} \dot{M}_{s,\alpha} = (\nu_{char} - \nu_{soot} - 1)\,\dot{\omega}_{pyr} - \dot{\omega}_{H_2O} - \dot{\omega}_{char} \tag{16}$$

$$\frac{d}{dt}(\alpha_s) = -\frac{1}{\rho_s}\dot{\omega}_{char} \tag{17}$$

$$\alpha_s \rho_s C_{p_s} \frac{dT_s}{dt} = h_{cond}\Sigma_s\,(T - T_s) - \sum_{\alpha} \dot{M}_{s,\alpha} h_{s,\alpha} + \Delta h_{char}\dot{\omega}_{char} + \frac{\alpha_s \sigma_s}{4}\left(J - 4n^2\sigma T_s^4\right) \tag{18}$$

where ν_{char} and ν_{soot} are respectively the stoichiometric coefficients of char and soot production from the thermal degradation of the solid fuel, ν_{ash} is the resulting fraction of ash (in the present calculation we have used $\nu_{char} = 0.45$, $\nu_{soot} = 0.015$ and $\nu_{ash} = 0.033$).
As previously pointed out, the radiation heat transfer includes the contributions of both fuel particles and soot.

Experimentally it has been shown that the size of soot particles during a forest fire ranges from 0.2 to $12\mu m$ [4]; in the present study a constant diameter $1\mu m$ is used. Therefore the soot field is completely defined from the soot volume fraction which verifies the following conservation equation:

$$\frac{\partial}{\partial t}(\alpha_g \rho_g f_v) + \frac{\partial}{\partial x}(\alpha_g \rho_g u_x f_v) = -\frac{\partial}{\partial x}(\alpha_g \rho_g u_x^{th} f_v) + \alpha_g \rho_g \dot{\omega}_{f_v} \tag{19}$$

$$\dot{\omega}_{f_v} = \frac{1}{\rho_{soot}}\left[\nu_{soot}\dot{\omega}_{pyr} - W_{Ox}\Sigma_s\right] \tag{20}$$

$$W_{Ox} = 120\left[\frac{k_A(T)P_{O_2}}{1 + k_z(T)P_{O_2}}\chi(T, P_{O_2}) + P_{O_2}\,(1 - \chi(T, P_{O_2}))\right] \tag{21}$$

where u_x^{th} is the mean thermophoretic velocity component in the x coordinate direction:

$$\widetilde{u_x^{th}} = -0.54\nu_g \frac{\partial \ln \widetilde{T}}{\partial x} \tag{22}$$

It can be noticed that the production rate of soot particles is represented as a fraction ν_{soot} of the mass loss rate due to pyrolysis; the oxidation of soot which can be assimilated to carbon particles is evaluated using the rate of oxidation of pyrolytic graphite [15, 10].
In Figure 2 (left), the mass loss curve computed using the present model is compared to TGA (thermogravimetric analysis) curve obtained with a heating rate of $10K/min$ [14]. The good agreement between

the experimental and the predicted mass losses validates the various physical constants included in our model used to describe the thermal degradation of fuel material. The corresponding evolutions of the mass fractions of solid fuel, water, and char are reported in Figure 2 (right). The desorption of water is complete at $T = 400K$ whilst the thermal degradation of solid fuel (wood) begins to be significative at $T = 500K$. The solid fuel sample is completely carbonized for $T = 650K$ and finally the ash formation occurs at $T = 710K$. These characteristic temperatures have been observed experimentally during the thermal decomposition of pine needles samples [16].

NUMERICAL RESOLUTION

The set of partial differential equations governing the physical behaviour of the gas mixture is solved using a Finite Volume method. To avoid numerical diffusion which can mask the physical diffusion and alter artificially the solution, we have used an Ultra-Sharp approach which combines a high-order upwind scheme with a flux limiter strategy [17]. The set of differential equations governing the evolution of the solid fuel bed is solved using a 4th order Runge-Kutta algorithm.
Numerical experiments have shown that the evaluation of mass loss is very sensitive to the number of grid points used to represent the fronts of water desorption and pyrolysis. This sensitivity results from the use of Arrhenius laws to calculate the corresponding reaction rates. We have noticed that the thickness of the degradation front is about $5mm$. If we consider that 5 points are necessary to represent accurately a degradation front, this criteria requires a mesh size of $1mm$. To reduce the computational time and to prepare a formulation which can be easily extended to 2D and 3D situations we have used an adaptative mesh strategy. This method consists in localizing the point in the fuel bed where the gradient of the mass fraction of solid fuel (Y_i^s) reaches its maximum which corresponds also to the region of fuel where the thermal degradation is the most intense. If the position of this degradation front has changed enough (more than $0.1mm$ for example) a new mesh is generated including a refinement of the grid size on both side of this front, and the numerical solution obtained at the previous time step is projected on the new mesh using a bilinear interpolation procedure [18].
The computed trajectory of the isotherm $T_s = 500K$ and the computed time evolution of the overall production rate of pyrolysis products ($CO + H_2O$) obtained with and without adaptive mesh refinement are shown in Figure 3. For this numerical test we have used a $0.2m$ long fuel bed (beyond a distance of $5cm$ from the end of the tube a steady state propagation is reached), a surface-to-volume ratio of $4550m^{-1}$ (pinus Pinaster) and a packing ratio is $\alpha_s = 0.05$. If the density of the solid fuel is $\rho_s = 680kg/m^3$ (dry value), the fuel loading is therefore $\overline{\rho_s} = \alpha_s \rho_s = 34kg/m^3$. The specific heat of the fuel bed is $C_{p_s} = 1380J/kg/K$. The fuel moisture content is fixed to $Y^s_{H_2O} = 0.08$. Calculations with and without adaptive mesh refinement are performed using a grid of 60 cells, and compared with a reference calculation performed with a grid of 200 cells. The trajectories of the isotherm $T_s = 500K$ (Figure 3 (top)) show that the calculation performed with a regular coarse mesh overestimates the rate of spread (ROS) of the combustion front. The curve reported in Figure 3 (bottom) shows that the rate of pyrolysis products obtained with the same mesh exhibits an unphysical oscillatory behaviour. The distribution of the solid phase temperature (evaluated at the center of each computational cell) is not represented with accuracy, introducing artificial variations in the evaluation of pyrolysis rates. The results obtained using the grid refinement strategy described previously, with the same number of grid points, show that this drawback can be completely corrected. The predicted ROS and the release rates of pyrolysis products obtained with this new algorithm are similar to those resulting from a reference calculation performed with 200 grid points.

NUMERICAL RESULTS AND DISCUSSION

A set of calculations has been performed for a $0.5m$ long fuel bed with a loading of $25kg/m^3$ ($\alpha_s = 0.0367$) using pine needles (Pinus Pinaster) as fuel. Incoming air velocity ranges from $2cm/s$ to $30cm/s$. Figure 4 shows the variations of the ROS with respect to the incoming air velocity U_{air}, in both the oxygen- and fuel-limited regimes. The stoichiometric oxidation of the combustible pyrolysis products (CO) corresponds to the boundary between these two regimes where ROS reaches a maximum. These two regimes have already been identified in the context of reverse flaming combustion or smolder propagation in permeable fuel bed [7, 19, 13], and for the downward flame spreading in an opposed forced flow [20]. The two combustion regimes are also observed in Figure 5 representing the pyrolysis reaction

rates ($CO + H_2O$) as a function of U_{air}. The distributions of CO, O_2 and CO_2 mass fraction in the gas mixture (Y_{CO}, Y_{O_2}, Y_{CO_2}) are reported in Figure 6 for two incoming air velocities (U_{air} = 7 and $25cm/s$). In the oxygen-limited regime (Figure 6 on the top) it is evident that the available oxygen is fully consumed by the homogeneous combustion and no heterogeneous combustion is observed. In the outflow, a significant mass fraction of gaseous fuel ($Y_{CO} = 0.12$) subsists. In the fuel-limited regime the oxygen is not completely consumed both homogeneous and heterogeneous reactions occur (see Figures 6 on bottom). The corresponding distributions of temperatures in the gas (T) and in the solid (T_s) phases are shown in Figure 7. The shift between T and T_s in front of the combustion zone is mainly due to heating of the fuel bed by radiative heat transfer.

CONCLUSION

A one dimensional numerical model has been developed to study the reverse combustion in a fuel bed of pine needles. A multiphase representation is used to describe the evolution of both phases. The simplified thermal degradation modelling used to describe water desorption, pyrolysis and char oxidation of solid particles of the fuel bed is quite satisfactory, reproducing the mass loss kinetic measured by thermogravimetry analysis. Calculations have been performed for various reverse air flow velocities U_{air}. Two combustion regimes have been predicted, an oxygen-limited and a fuel-limited regime. An experimental study is in progress to measure the ROS in a fuel bed of pine needles in a tube and then validate our multiphase formulation.

ACKNOWLEDGMENT

The European Economic Commission is gratefully acknowledged for providing partial funding for this research in the frame of the EFAISTOS project.

References

[1] R.O. Weber, "Modeling fire spread through fuel bed", in Prog. Energy Combust. Sci., 17:67–82, 1990.

[2] W.M. Pitts, "Wind effects on fires", in Prog. Energy Combust. Sci., 17:83–134, 1991.

[3] T.J. Ohlemiller, "Modeling of smoldering combustion propagation", in Prog. Energy Combust. Sci., 11:277–310, 1985.

[4] A.M. Grishin, Mathematical modeling of forest fires and new methods of fighting them, Publishing house of the Tomsk University, Tomsk, Russia. Ed. by F. Albini, 1997.

[5] M. Xie and X. Liang, "Numerical simulation of combustion and ignition-quenching behavior of a carbon packed bed", in Combust. Sci. and Technol., 125:1–24, 1997.

[6] R.R. Lin, A Transport Model for Prediction of Wildfire Behavior, PhD thesis, Los Alamos National Laboratory, 1997.

[7] M. Larini, F. Giroud, B. Porterie, and J.C. Loraud, "A multiphase formulation for fire propagation in heterogeneous combustible media", in Int. J. Heat Mass Transfer, 41:881–897, 1998.

[8] G. Lauriat, "Combined radiation-convection in gray fluids enclosed in vertical cavities", n J. Heat Transfer, 104:609–615, 1982.

[9] T. Fusegi and B. Farouk, "Laminar and turbulent natural convection-radiation interactions in a square enclosure filled with a nongray gas", in Numerical Heat Transfer, Part A, 15:303–322, 1989.

[10] C.R. Kaplan, C.R. Shaddix, and K.C. Smyth, "Computations of enhanced soot production in time-varying ch_4/air diffusion flames", in Combust. Flame, 106:392–405, 1996.

[11] F.P. Incropera and D.P. DeWitt, Fundamentals of heat and mass transfer, John Wiley and sons (4th Edition), 1996.

[12] T. Kashiwagi and H. Nambu, "Global kinetics constants for thermal oxidative degradation of a cellulosic paper", in Combust. Flame, 88:345-368, 1992.

[13] M. Fatehi and M. Kaviany, "Adiabatic reverse combustion in a packed bed", in Combust. Flame, 99:1-17, 1994.

[14] C. Vovelle, H. Mellottee, and R. Delbourgo, "Kinetics of the thermal degradation of cellulose and wood in inert and oxidative atmospheres", in 19th Symposium. (International) on Combustion, The combustion Institute, pages 797-805, 1982.

[15] J. Nagle and R.F. Strickland-Constable, "Oxidation of carbon between $1000-2000°c$, in Proceedings 5th Conference on Carbon, volume 1, pages 154-164, 1962.

[16] C. Moro, "Etude de la decomposition d'echantillons vegetaux en fonction de la temperature", Technical report, INRA Equipe de Prevention des Incendies de Foret PIF9702, 1997.

[17] B.P. Leonard and S. Mokhtari, "Beyond first-order upwinding: the ultra-sharp alternative for non-oscillatory steady-state simulation of convection", in Int. J. Numerical Methods Engineering, 30:729-766, 1990.

[18] M.D. Smooke and M.L. Koszykowski, "Two-dimensional fully adaptive solutions of solid-solid alloying reactions", in J. Comput. Physics, 62:1-25, 1986.

[19] T.J. Ohlemiller and D.A. Lucca, "An experimental comparison of forward end reverse smolder propagation in permeable fuel beds", in Combust. Flame, 54:131-147, 1983.

[20] A.C. Fernandez-Pello, S.R. Ray, and I. Glassman, "Downward flame spread in an opposed forced flow", in Combust. Sci. and Technol., 19:19-30, 1978.

Figure 1: Reverse combustion front traveling through a fuel bed of pine needles.

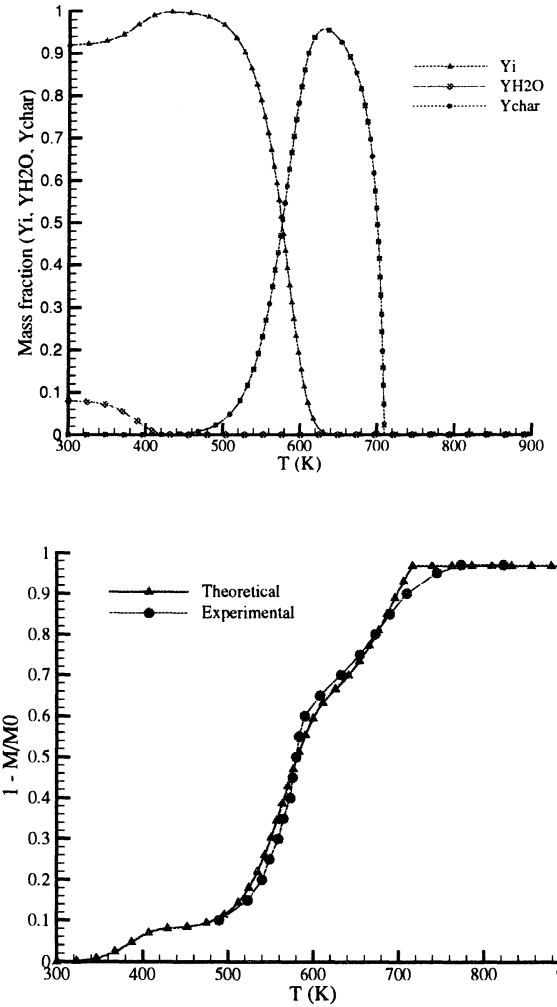

Figure 2: Computed evolutions of the solid fuel, water and char mass fractions (top) and mass loss (bottom) of a wood sample for a heating rate of $(10K/min)$.

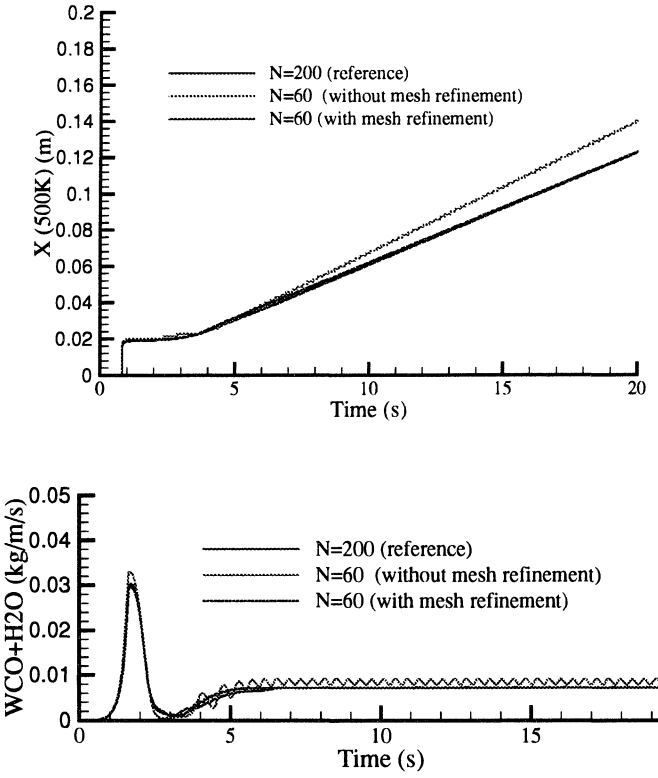

Figure 3: Reverse combustion in a fuel bed of pine needles. Time evolutions of the isotherm $T_s = 500K$ (top) and $CO + H_2O$ production rate (bottom) computed with and without adaptive mesh refinement.

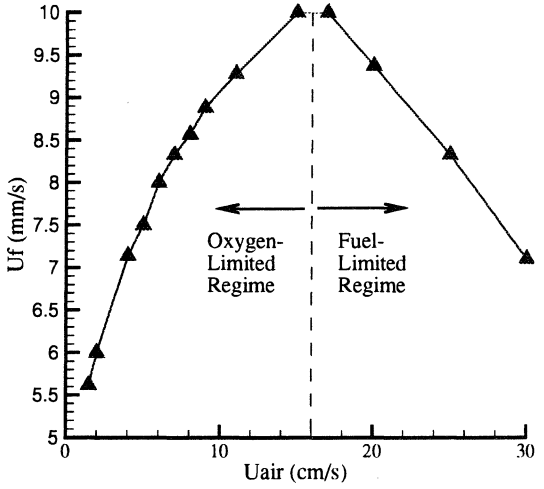

Figure 4: Rate of spread (ROS) as a function of incoming air velocity.

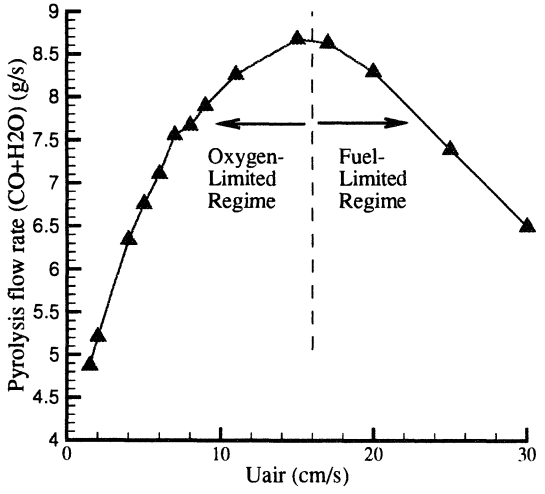

Figure 5: Pyrolysis reaction rate ($CO + H_2O$) as a function of incoming air velocity.

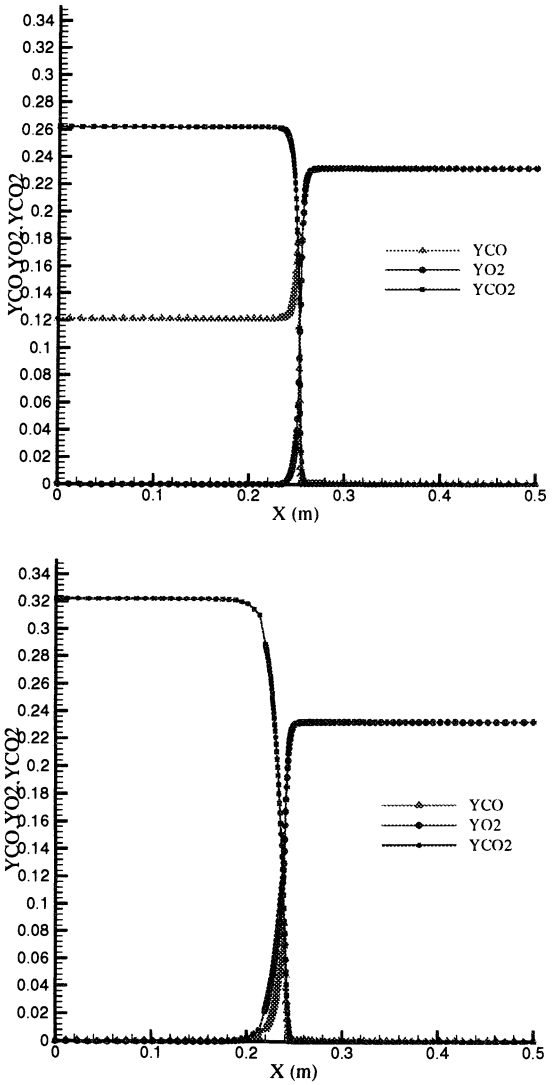

Figure 6: Computed mass fractions of CO, O_2 and CO_2 for incoming air velocity of $7cm/s$ (top) and $25cm/s$ (bottom).

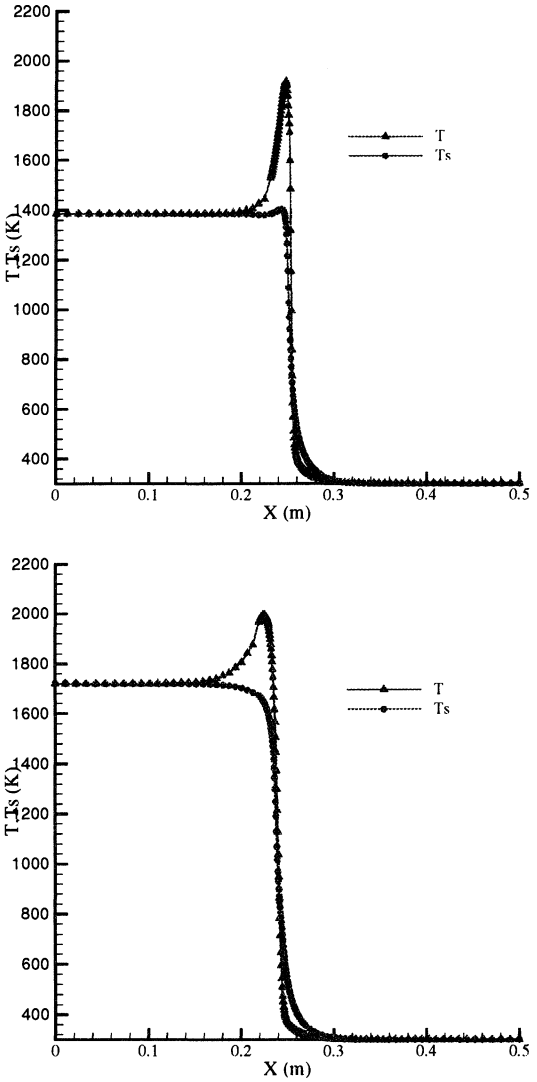

Figure 7: Gas and solid phase temperatures for incoming air velocity of $7cm/s$ (top) and $25cm/s$ (bottom)